Altered systemic bioenergetic reserve in chronic kidney disease predisposes hearts to worse functional outcomes

Authors: Megan Young[1], Malene Aastrup[2], Nikayla Patel[1], Fenn Cullen[1], Esben S.S. Hansen[2], James E. Clark[3], Thomas R. Eykyn[4], Michael Vaeggemose[2,5], Ana Vujic[6], Loucia Karatzia[1], Ladislav Valkovič[7,8], Jack J.J.J. Miller[2], Niels H. Buus[9], Christoffer Laustsen[2], Magdi M. Yaqoob[1], Dunja Aksentijevic[1]*

Affiliations:

[1]William Harvey Research Institute, Barts and the London Faculty of Medicine and Dentistry, Queen Mary University of London; London, United Kingdom

[2]The MR Research Centre, Department of Clinical Medicine, Aarhus University; Aarhus, Denmark

[3]The Rayne Institute, School of Cardiovascular and Metabolic Medicine and Sciences, Faculty of Life Sciences & Medicine, King's College London; London, United Kingdom

[4]Department of Imaging Chemistry and Biology, School of Biomedical Engineering and Imaging Sciences, King's College London; London, United Kingdom

[5]GE HealthCare; Brondby, Denmark

[6]Department of Medicine, University of Cambridge; Cambridge, United Kingdom

[7]Oxford Centre for Clinical Magnetic Resonance Research (OCMR), University of Oxford; Oxford, United Kingdom

[8]Department of Imaging Methods, Institute of Measurement Science, Slovak Academy of Sciences; Bratislava, Slovakia

[9]Department of Renal Medicine, Aarhus University; Aarhus, Denmark

*Corresponding author. Email: d.aksentijevic@qmul.ac.uk

One Sentence Summary: Perturbations of systemic metabolism precede and exceed severity of cardiac metabolic changes in chronic kidney disease.

Abstract:

Chronic kidney disease (CKD) is the tenth biggest killer worldwide and is projected to be the fifth leading cause of mortality by 2040. CKD is an inherently systemic disease with progressive deterioration of kidney, muscle, and liver function creating a vicious cycle of comorbidity. However, whether systemic energetic deficiency in CKD contributes to cardiac dysfunction of the uraemic cardiomyopathy remains unknown. Using two pre-clinical renal failure models of different aetiology in rats (4-week 0.75% adenine diet and 12-week post-partial nephrectomy) we investigated both cardiac and systemic metabolic remodelling in CKD. In addition to significant uraemia, anaemia and alterations in exogenous plasma substrate homeostasis, non-targeted ^{1}H NMR spectroscopy metabolomic profiling of peripheral tissues (skeletal muscle, liver, kidneys) revealed extensive metabolic alterations and changes in bioenergetic reserve in both experimental CKD models. Similarly, ^{31}P magnetic resonance spectroscopy assessment of the exercising lower leg muscle of CKD human patients identified systemic bioenergetic deficiency. During exercise CKD patients were unable to utilise the energetic capacity to the same extent as healthy controls. Both experimental CKD models developed mild cardiac dysfunction, however metabolic remodelling was less severe than that of systemic organs. Upon challenge with 25-minute total global ischemia, CKD hearts from both experimental models had poorer functional outcome. Thus, in CKD perturbation of systemic metabolism precedes and exceeds severity of cardiac metabolic changes. Prevention of systemic metabolic derangement in CKD may be a new therapeutic approach to improve cardiac functional outcomes in CKD.

Main Text:

INTRODUCTION

Chronic kidney disease (CKD) is a progressive disease with a decline in renal function leading to kidney failure. CKD is a global public health emergency affecting 840 million people and a leading cause of mortality (*1*). 10% of the UK population (7.2 million) are estimated to suffer from CKD, carrying an annual UK economic burden of £7 billion (*2*). Based on the current projected rate of increase in CKD patient numbers, this public health cost is forecast to double over the next 10 years with the UK NHS dialysis capacity needing to grow by 400% to meet essential demand (*2*).

For many CKD patients the risk of developing cardiovascular disease is higher than progression to kidney failure (*3*). Uraemic cardiomyopathy is a distinct pathology characterised by diastolic dysfunction, left ventricular hypertrophy (LVH), fibrosis and maladaptive changes in cardiac metabolism (*4*). CKD hearts have alterations in metabolic substrate utilization preference, alongside impaired cardiac energetic reserve and an inability to respond to oxidative stress (*5, 6*). In severe CKD, cardiac complications can progress into heart failure (HF), largely with preserved ejection fraction (*4, 7*).

However, CKD is an inherently systemic disease, and renal insufficiency causes dysfunction of multiple other organs (*8*). Extensive systemic metabolic alterations occur in CKD including insulin resistance associated with increased fatty acid catabolism, muscle wastage, as well as perturbed kidney metabolism (*9*). CKD progression generates a high-risk clinical phenotype which includes inflammation, malnutrition, altered activity of the autonomic and central nervous systems, cardiopulmonary, vascular and bone disease (*8*). Skeletal muscle metabolism has significant implications for physical function, quality of life, and overall health in CKD patients. Skeletal muscle is a crucial organ for metabolic homeostasis, playing an essential role in insulin sensitivity, protein metabolism, and energy expenditure. However, individuals with CKD often experience alterations in muscle metabolism that can exacerbate their clinical condition and

contribute to cachexia. Furthermore, reduced mass and strength contribute to fatigue suffered by CKD patients which notably impairs quality of life (*10*).

Alterations in renal clearance can significantly impact liver function and vice versa, creating a complex interrelationship that can exacerbate CKD patient outcomes. Declining kidney function triggers altered carbohydrate metabolism, dyslipidemia, and abnormalities in bilirubin metabolism (*11*). The liver regulates glucose metabolism, lipid synthesis, and detoxifies harmful products of protein metabolism, including urea and creatinine. Thus, hepatic-renal interorgan cross talk is critical as both organs are vital to systemic metabolic homeostasis and detoxification (*12*). As renal function declines, the accumulation of uremic toxins can overwhelm the liver's capacity to metabolize and eliminate these toxic substances, leading to liver pathologies (*13*). The resultant metabolic syndrome commonly observed in CKD patients contributes to further deterioration of both liver and kidney function, creating a vicious cycle of comorbidity (*13*).

Given that the driving factors for uraemic cardiomyopathy are multifactorial, it remains unknown whether crosstalk between systemic metabolic remodelling in CKD could be contributing to uraemic cardiomyopathy. Previous work in CKD has shown that energetic reserve in skeletal muscle mirrors cardiac energetic reserve (*6*), highlighting the interconnecting cross-talk between two physiological systems. Therefore, investigation into systemic metabolic changes in CKD may help to identify the association with pathophysiology of uraemic cardiomyopathy.

Utilising two animal models of different CKD aetiology in rats (4-week 0.75% adenine diet and 12-week partial nephrectomy), we investigated both cardiac and systemic metabolic alterations that develop in response to progressively declining renal function. We show in both experimental models that renal insufficiency, irrespective of aetiology, results in cardiometabolic remodelling predisposing CKD hearts to poor ischemia-reperfusion outcome. Non-targeted metabolomic profiling of liver, muscle and kidney by high resolution ^{1}H nuclear magnetic resonance spectroscopy (NMRS) identified extensive metabolic changes and reduction of systemic bioenergetic reserve in both animal models. This pre-clinical CKD

outcome was recapitulated in human subjects. Bioenergetic capacity of the lower leg muscle of human CKD patients was assessed during exercise using phosphorus magnetic resonance spectroscopy (^{31}P MRS). Unlike healthy controls, CKD patients were unable to utilise their systemic energetic capacity to the same extent thus preventing maximal force generation. By elucidating the relationship between kidney dysfunction and systemic metabolism, we aim to contribute to a more comprehensive understanding of this critical aspect of CKD management.

RESULTS

CKD phenotype and cardiometabolic remodelling in CKD animal models

Adenine diet induced CKD

0.75% adenine diet CKD induction protocol in Wistar rats led to renal dysfunction evident from increased plasma levels of creatinine and urea compared to control diet (Fig. 1A, B) as well as anaemia (Fig. 1C). Given the adenine CKD model is characterized by the absence of hypertension (*14*), there was no increase in LVH index (Fig. 1D) or increases in LV wall thickness (Table S2). Changes in left ventricular internal diameter in diastole (LVID,d) and end diastolic volume (EDV) (Fig. 1E, F) reflect mild ventricular remodelling and compensatory increases in contractility to maintain ejection fraction (Fig. 1G). There is no evidence of congestive heart failure and lung oedema in adenine CKD (Fig. S2A). mRNA expression of BNP (Fig. 1H) as well as PCr/ATP ratio (Fig. 1I) were comparable between the adenine CKD heart and controls. ^{1}H NMR spectroscopy assessment of adenine CKD myocardial metabolome revealed perturbed fatty acid metabolism intermediates: increased acetyl carnitine and reduced carnitine and phosphocholine (Fig. 1J, Fig. S3). Furthermore, adenine diet-induced CKD caused marked changes in cardiac lipid content (Fig. S4). Expression of fatty acid transporter CD36 was increased in adenine CKD hearts, alongside a decreased expression of insulin-dependent glucose transporter Glut4 (Fig. 1H). In terms of plasma metabolic profile (Table 1), adenine diet CKD animals had reduced circulating levels of glucose and insulin compared to control.

Partial nephrectomy (PN) CKD

Two-stage PN surgery induced a CKD phenotype characterized by renal dysfunction (elevated plasma levels of creatinine and urea – Fig. 2A, B), anaemia (Fig. 2C) and cardiometabolic remodelling. In addition to uraemia and anaemia, hypertension is present in PN model of CKD from the onset (*15-17*). 12-weeks of CKD progression led to pathological ventricular remodelling observed from an increase in LVH index (Fig. 2D). *In vivo* cardiac assessment identified changes in cardiac wall thickness and decreased internal diameter (Fig. 2E, F). Furthermore, elevated mRNA expression of BNP (Fig. 2H) is indicative of developing heart failure however in the absence of reduced ejection fraction (Fig. 2G). Assessment of circulating metabolites showed a decline in plasma glucose levels in PN CKD (Table 2). ^{1}H NMR myocardial metabolomic profiling of PN CKD identified changes in amino acid metabolism (Fig. 2J) without alterations in the expression of metabolic transporters (CD36 and Glut4, Fig. 2H). However, cardiac energy reserve was impaired as PCr/ATP ratio was significantly reduced (Fig. 2I).

Model specific responses to CKD induction

Adenine diet and PN CKD models have distinct aetiology resulting in differences in the CKD phenotype induced. The adenine CKD model has a more severe perturbation of renal function, as well as significantly impaired systemic glucose homeostasis (altered circulating glucose, insulin) not seen in the PN CKD model (Fig. S5). The cardiac phenotype also differs between the two CKD models, with evidence of cardiac hypertrophy in the PN CKD model but not seen in the adenine model. Furthermore, the cardiac metabolomic changes differ between CKD models (Fig. S6A), and the PN CKD model had a more robust decline in cardiac PCr/ATP ratio.

CKD increases susceptibility to cardiac ischemia reperfusion injury

Given the evidence of altered cardiometabolic profile of CKD hearts, we examined the response to ischemia and reperfusion. When stressed by a period of 25-minute total global normothermic ischemia followed by 25-minute reperfusion, both adenine and PN CKD hearts display poor outcomes (Fig. 3). Given the unaltered PCr/ATP ratio, adenine CKD hearts do show signs of improved recovery during the immediate

onset of reperfusion, however this is not sustained (Fig. 3). At the end of 25-minute reperfusion, adenine and PN CKD heart LVDP recovered 8.02% and 9.75% respectively compared to 50.42% control hearts recovery (Fig. 3).

CKD development leads to systemic metabolic alterations

Skeletal muscle

Skeletal muscle damage was evident in adenine CKD animals and to a lesser extent in PN CKD. Adenine CKD was associated with increased circulating levels of creatine kinase (Fig. 4B), as well as a reduction in body weight (Fig. 4A) indicative of muscle wastage. The metabolomic profiling of skeletal muscle from adenine CKD animals revealed decline in energy reserve with reduced PCr/ATP accompanied by increased amino acids concentrations (aspartate, alanine, glutamine, glutamate, Fig. 4D). The PN CKD model was characterized by doubling of circulating creatine kinase (Fig. 4C) and changes in skeletal muscle acetyl carnitine and amino acid profile (Fig. 4E).

Kidney

As expected with induction of CKD, kidney morphology function and metabolomic profile were significantly impacted. Renal dysfunction is evident in both CKD models with increased plasma levels of creatinine and urea (Fig. 1A-B, 2A-B). In the adenine CKD model both kidneys are intact accompanied by significant and strikingly visible kidney hypertrophy (significant increase in both left and right kidney weight, Fig. 5A- C). Kidney morphology is harder to compare with weights in the PN CKD model given the surgical resection, although there is visual evidence of compensatory hypertrophy in the 1/3 remaining kidney.

Both experimental models of CKD had marked changes in the metabolomic profile of kidney tissue, to a greater extent in the adenine model (Fig. 5D, E). In the adenine CKD model overt metabolic changes were observed with 20 changed out of 32 metabolites studied, including reduction in energetics (reduced ATP,

Fig. 5D). Energetics were unaffected in the PN CKD model (Fig. 5E). There are similarities in the kidney metabolic remodelling between both CKD models including increased amino acids (Fig. 5D, E).

Liver

The liver phenotype of both CKD models included reduction in liver weight (Fig. 6A, B). There were changes in the liver metabolomic profile of adenine CKD animals including a reduction in taurine (Fig. 6C). In PN CKD, changes in the metabolomic profile included changes in energy reserve (Fig. 6D).

^{31}P MRS assessment of exercising leg muscle of CKD patients identifies functional bioenergetic impairment

Given the finding of perturbed metabolism in the peripheral tissues of the CKD animal models, we sought to measure the energetic reserve in skeletal muscle of CKD patients when challenged with exercise. The demographic and clinical characteristics of the CKD patients and healthy control study participants is shown in Table 3. ^{31}P MRS was obtained from the tibialis anterior muscle of healthy controls and CKD patients at baseline, during exercise, and during the 10-minute recovery period (Fig. 7A). The depletion of PCr can be observed across the exercise period, followed by resynthesis during recovery (Fig. 7B-C). At baseline, CKD patients had a comparable PCr/ATP ratio to healthy controls (Fig. 7D), however the utilisation of PCr during exercise was 35% lower in the CKD patient group (ΔPCr, Fig. 7E). Furthermore, we examined the maximum torque generation during exercise and found the CKD patient group generated significantly lower force than healthy controls (Fig. 7F). Whilst the muscle PCr utilisation is comparable between CKD patients and controls when torque generation is accounted for (Fig. 7G), mitochondrial capacity (Qmax) is significantly decreased (Fig. 7H) alongside a decreased initial rate of PCr resynthesis (Fig. 7I). The overall PCr recovery indicated by Tau as well as pH was comparable between CKD patients and healthy controls (Fig S7A, B).

DISCUSSION

Given the systemic nature of CKD and metabolic crosstalk between organs, we investigated both the cardiac and systemic metabolic signature of two CKD animal models with two distinct aetiologies. Moreover, we assessed metabolic capacity of skeletal muscle of human CKD patients. This study identified that CKD regardless of aetiology leads to cardiometabolic remodelling and increased susceptibility to ischemia reperfusion injury. However, changes in systemic metabolomic profile (muscle, liver, kidney) precede and exceed severity of cardiac metabolic remodelling. We also show that despite comparable energetic capacity to healthy controls at rest, CKD patients have an inability to utilise their muscle energetic reserve. Therefore, we demonstrate inability of skeletal muscles in CKD patients to respond to a metabolic stress.

We have previously shown that experimental uraemia induced by PN leads to development of anaemia, hypertension, LVH, altered substrate utilization collectively resulting in cardiac energetic impairment (*5, 6, 15-18*). However, cardiometabolic remodelling is less extensively reported for the adenine-diet induced CKD experimental model. Adenine-diet induced CKD is of distinct aetiology to PN and induces a more severe form of CKD with the absence of hypertension (*14*). The absence of pressure overload is evidenced by the lack of LVH. Observed cardiac functional changes are suggestive of compensatory functional response to maintain ejection fraction under hyperdynamic confounders including severe anaemia. Metabolic profile of adenine-diet induced CKD cardiomyopathy was characterized by altered expression of insulin-responsive myocardial glucose and fatty acids transporters, altered myocardial fatty acid metabolism intermediates accompanied by impaired systemic glucose homeostasis (circulating hypoglycaemia and hypoinsulinaemia). However, unlike the PN CKD model, adenine-diet induced CKD hearts had preserved myocardial energy reserve and no evidence of HF development.

Cardiac metabolism is firmly intertwined with cardiac function, providing a continuous supply of energy to meet demand (*4*). Therefore, unsurprisingly, changes in cardiac metabolism are a hallmark of the development of uraemic cardiomyopathy (*4, 7*). Historically, PN CKD hearts have been shown to preferentially switch energy substrate usage towards glycolysis over fatty acid metabolism, concurrent with

a decline in energy reserve (*5, 6, 18*). Although there are no extensive changes in intermediate myocardial metabolite concentration in PN CKD, alterations in myocardial amino acid profile are indicative of metabolic adaptation to maintain ATP supply (*19*). However, these metabolic adaptations were insufficient to maintain a healthy cardiac phenotype as reduced PCr/ATP and elevated BNP levels are indicative of progression into HF with a preservation of ejection fraction.

Myocardial ischemia is a major cause of death in CKD patients (*20*). Hearts from models of experimental uraemia have been shown to have increased susceptibility to mitochondrial permeability transition, which contributes to increased susceptibility to ischemia reperfusion injury (*21*). We found that irrespective of the renal failure aetiology and the state of energy reserve of the heart, the presence of CKD with its multifaceted pathophysiology enhances the myocardial susceptibility to ischemic stress (*22*). Given the cardiometabolic remodelling in CKD, it is unsurprising CKD hearts have increased susceptibility to ischemia reperfusion injury resulting in larger infarct size (*21*). Adenine CKD hearts show some initial signs of recovery during reperfusion reflective of the preserved baseline energetics but ultimately recovery during reperfusion is poor. Thus, any underlying cardiac metabolic changes in CKD may be sufficient to maintain energetic reserve under basal conditions, but the ability to respond to stress is ultimately impaired. This is line with previously reported enhanced dobutamine stress susceptibility in PN CKD cardiomyopathy (*6*).

Metabolic crosstalk between organs has been highlighted in HF of various aetiology as well as in CKD (*23*), however metabolomic profiling of organs in experimental CKD has not been reported. We examined the systemic metabolic signature in CKD by assessing the metabolism of peripheral tissues and exogenous (circulating) substrate supply. Here we show extensive changes in metabolomic profile of skeletal muscle, kidney and liver. Given the multifaceted nature of CKD, changes in the systemic energetic reserve and metabolism are likely to be intertwined with the poorer cardiovascular outcomes we observed.

Muscle wastage, fatigue and poor physical performance are common in CKD, and a major debilitating feature of the disease impacting patients' quality of life (*24, 25*). Previous work has shown skeletal muscle energetic reserve correlates with cardiac energetic decline in experimental uraemia, highlighting the metabolic and functional relationship between organs (*6*). Furthermore, in the calf muscle of haemodialysis patients, ATP supply via oxidative metabolism is impaired and compensated for by an increase in anaerobic glycolysis (*26*).

Interestingly we found a muscle specific decline in PCr/ATP ratio in the adenine diet-induced CKD model, without accompanying decline in cardiac energetic reserve. This may suggest that in CKD skeletal muscle energetic impairment precedes detrimental cardiac changes. We investigated this relationship further in human CKD patients. We found that despite comparable baseline energy reserve, during exercise CKD patients were unable to utilise PCr to the same extent as healthy controls. Furthermore, torque generation was lower in CKD patients versus healthy controls. Given the relationship between CKD, muscular wastage and fatigue this may be reflected in reduced capacity for muscle force generation observed. Our findings are in line with previous reports that CKD patients have reduced peak oxygen capacity, skeletal muscle mitochondrial capacity, reduced mitochondrial number, mitochondrial dysfunction and increased superoxide generation (*27-29*). However, the utilisation of PCr relative to the torque generation was comparable. Therefore, the energetic impairment in skeletal muscle of CKD patients is not solely governed by the availability of PCr nor by a need to utilise greater amounts of energy to produce the same level of force. The limiting factor appears to be an inability to utilise the available energy reserve, leading to the development of fatigue. Understanding the intricacies of muscle metabolism in CKD is essential for developing effective therapeutic approaches aimed at preserving muscle mass and function, ultimately improving patient outcomes.

Amongst the multiple systemic complications in CKD is the interplay between kidney and liver (*12*). Decline in kidney function impacts the reabsorption and therefore availability of metabolites within the body. CKD led to development of severely perturbed kidney metabolism in both experimental models.

Irrespective of CKD induction protocol, there were similarities in the renal metabolic reflecting the underlying uraemia. In the adenine-diet CKD model kidneys are uniformly and severely injured due to adenine deposits in the kidney (*14*) which led to reduced energy reserve, whereas PN involves surgical resection to reduce functional kidney capacity (*17*). However, whilst the remnant portion of kidney is hypertrophied in the PN CKD model to compensate for reduced renal capacity, it had normal energy reserve.

Development of CKD also affects the liver with whole-body consequences as liver is a central systemic metabolic regulator. CKD is associated with higher prevalence of liver metabolic diseases such as cirrhosis and non-alcoholic fatty liver disease as two pathologies share several risk factors, including insulin resistance, oxidative stress, inflammation alongside an increased prevalence of cardiovascular disease (*30, 31*). These hepatic pathologies can exacerbate the symptoms of CKD that complicate therapeutic management strategies. Furthermore, liver metabolic alterations in CKD can influence drug metabolism and efficacy, further straining liver function. Our study identified extensive alterations in liver redox, energy reserve and elevation of the lipid metabolism intermediates. Furthermore, a reduction in taurine was noted in liver from adenine CKD models, a key regulator of hepatic oxidative stress and fatty liver disease (*32*). Improved understanding of hepatic-renal interplay can inform better therapeutic strategies, enhance monitoring protocols, and pave the way for interventions that can mitigate the adverse effects of CKD on overall metabolic health.

CKD is a complex disease with many associated risk factors and comorbidities. Crosstalk between organs has been identified in HFpEF of different aetiologies (*33*) and likely contributes to the systemic nature of CKD including the development of uraemic cardiomyopathy. There have been suggestions of a role for inflammation in this crosstalk (*34*), in addition to increased oxidative stress which may be driving the cardiovascular phenotype. Here we suggest there is a role for changes in systemic metabolism and bioenergetic reserve that is interlinked to the cardiometabolic remodelling in uraemic cardiomyopathy. This study expands upon previous research into cardiometabolic remodelling in CKD by utilising the adenine

diet model in addition to PN to induce chronic renal dysfunction. It shows the metabolic signature in CKD includes heart as well as liver, kidneys, muscles and plasma. This is supported by findings of impaired energetic utilisation in CKD patients when stressed with exercise, which mirrors the impaired response to cardiac ischemic stress we report in the experimental CKD models. Therefore, we suggest the severe systemic metabolic alterations observed in CKD and compromised energetic reserve, alongside cardiometabolic remodelling, contribute to poor cardiovascular outcomes in CKD. Moreover, therapeutic targeting and prevention of systemic metabolic derangement may be a new approach to ameliorate aberrant cardiac remodelling in CKD. Improved understanding of organ interplay can inform better therapeutic strategies, enhance monitoring protocols, and pave the way for interventions that can mitigate the adverse effects of CKD on overall metabolic health.

By elucidating the pathophysiological mechanisms at play within this multifaceted syndrome, we may improve the quality of life for patients affected by CKD and reduce the burden of liver-related complications.

MATERIALS AND METHODS

Animals

For all experiments in this study, 250 g male Wistar rats (n=48) were purchased from Charles River Laboratories (UK). Animals were housed in individually ventilated cages and maintained under controlled temperature (22 ± 2 °C) on a 12:12 h light and dark cycles with access to standard chow diet (irradiated Labdiet 5LF2 – EURodent Diet 14%) and water *ad libitum.* Enrichment was provided in the form of tunnels and chew sticks. All animal experiments were in keeping with the UK Home Office Animals (Scientific Procedures), 1986. At the end of the experimental model induction protocol, all animals were humanely sacrificed by phenobarbital I.P. injection.

Experimental models of chronic kidney disease

Partial nephrectomy

Partial nephrectomy (PN) CKD was induced using an established two-stage surgical procedure for a period of 12 weeks (n=13) (*5, 14, 17*). Controls were sham operated (n=7) by removing the renal capsule and replacing the intact kidney. At 24 h after the second procedure, animals were housed individually, weighed weekly and had unlimited access to water.

Adenine diet

In a separate cohort of animals, CKD was induced using dietary manipulation with 0.75% adenine in standard rat chow diet (n=15) with controls fed standard rodent diet (n=8) for 4 weeks (Lillico Biotechnology). Adenine diet induction of CKD leads to rapid onset kidney damage as changes occur from 6 days to 4 weeks (*35*).

Transthoracic echocardiography

For the assessment of cardiac function, M-mode-echocardiography was performed in control diet, sham control, adenine diet induced-CKD and PN CKD animals. Anaesthesia was induced with 5% isoflurane and maintained at 1.5-2% for the duration of the procedure. Before assessment of cardiac function, fur was removed from the chest area to allow accurate assessment of cardiac function and rats were allowed to stabilize for at least 10 minutes. Body temperature was maintained at 37 °C. Echocardiography images were recorded using a Vevo 770 imaging system (Visualsonics, Canada). Percentage ejection fraction (EF) was calculated from the M-mode measurements in the parasternal short axis view at the level of the papillary muscles.

Biochemical analysis

The tissues (liver, skeletal muscle, heart, kidney, lungs) and blood were rapidly collected upon termination and snap frozen in liquid N_2 using Wollengerber tongs (*36*). The frozen heart weight was normalised to tibia length to assess the degree of cardiac hypertrophy (heart weight:tibia length). Lung weights were recorded and dried to a constant weight to determine wet lung: dry lung weight ratio. Blood samples, taken

from the thoracic cavity at the time of sacrifice were centrifuged at 3000 rpm. All samples were stored at -80°C until biochemical analysis. Plasma samples were analysed by the Clinical Biochemistry Laboratory at the Addenbrookes Hospital, Cambridge.

qPCR

RNA was isolated using RNeasy Fibrous Tissue Kit (Qiagen) according to the manufacturer's instructions. RNA quantity and quality was assessed using NanoDrop ND-1000 spectrophotometer and only RNA with 260/280 >1.8 was used for analysis. 1µg total RNA was reverse transcribed using High-Capacity cDNA Reverse Transcription Kit (Applied Biosystems). For qPCR, gene specific primer sequences are shown in Supplementary Table 1. qPCR reactions were performed in triplicates using Brilliant III Ultra-fast SYBR Green qPCR Master Mix with low ROX (Agilent) according to the manufacturer's instructions with the following cycling conditions: 95ºC for 3 min, 40 cycles of 95ºC for 5 sec and 60ºC for 60 sec using QuantStudio 5 (Applied Biosystems). The relative quantity of each gene was calculated using ΔΔCT method with 36B4 as endogenous control.

Langendorff heart perfusions

Rats were sacrificed by pentobarbital I.P. injection, hearts rapidly excised, cannulated and perfused in Langendorff mode as previously described (*19, 37*). Krebs-Henseleit (KH) perfusion buffer was continuously gassed with 95% O_2/5% CO_2 (pH 7.4, 37 °C) containing (in mM): NaCl (116), KCl (4.7), $MgSO_4 \cdot 7H_2O$ (1.2), KH_2PO_4 (1.2), $NaHCO_3$ (25), $CaCl_2$ (1.4), and enriched with metabolites [glucose (5), intralipid (0.4), sodium L-lactate (1), sodium pyruvate (0.1), L-glutamic acid monosodium salt monohydrate (0.5), 5 mU l^{-1}insulin] (NovoRapid insulin, Novo Nordisk, Denmark). After 20 min of equilibration, hearts were subject to 25 min of global normothermic ischemia (37°C) and 25 min of reperfusion.

Metabolomic analysis using ^{1}H Nuclear Magnetic Resonance (NMR) Spectroscopy

Snap frozen and pulverized tissue [liver, skeletal muscle (gastrocnemius and soleus), kidney, heart] was analysed using ^{1}H NMR high resolution spectroscopy as previously described (*36, 38*). Pulverised tissue samples (~100 mg) were subject to methanol/water/chloroform phase extraction. ^{1}H nuclear magnetic resonance spectra were acquired using a vertical-bore, ultra-shielded Bruker 14.1. Tesla (600 MHz) spectrometer with a BBO probe at 298K using the Bruker noesygppr1d pulse sequence. Acquisition parameters were 128 scans, 4 dummy scans and 20.8 ppm sweep width, acquisition time of 2.6s, pre-scan delay of 4s, 90° flip angle and experiment duration of 14.4 minutes per sample. TopSpin (version 4.0.5) software was used for data acquisition and for metabolite quantification. FIDs were multiplied by a line broadening factor of 0.3 Hz and Fourier-transformed, phase and automatic baseline-correction were applied. Chemical shifts were referenced to the TSP signal. Metabolite peaks of interest were initially integrated automatically using a pre-written integration region text file and then manually adjusted where required. Assignment of metabolites to their respective peaks was carried out based on previously obtained in-house data, confirmed by chemical shift and using Chenomx NMR Profiler Version 8.1 (Chenomx, Canada). Peak areas were normalized to the total metabolite peak area. Quantification of glycogen was performed by ^{1}H magnetic resonance, giving a measure of the concentration of glucose monomers that are present in the observed peak. Being a large macromolecule, with possible differences in the mobility of glycosyl units, glycogen has been reported to be fully visible by MRS. The modified dual-phase Folch extraction method used for separating aqueous and lipid metabolites was not optimized for the extraction of glycogen, however all samples underwent the same extraction procedure allowing between treatment group comparison (*36*).

Human Subjects

Ten patients (8 males, 2 females) with non-diabetic CKD stage 3b and 4, a mean age of 61 years and a mean estimated glomerular filtration rate of 27 ml/min/1.73m^{2} were recruited for the ^{31}P dynamic MRS study. The clinical characteristics of the patient cohort can be found in Table 3. The control arm consisted of 5 healthy volunteers (4 males, 1 female) with a mean age of 54 years and normal renal function. The

study protocol was approved by the Ethics Committee of Central Denmark (ref. 1-10-72-145-23) and all methods were performed in accordance with their guidelines and regulations. All subjects provided written consent prior to participation.

Assessment of the human tibialis anterior muscle bioenergetic reserve by dynamic ^{31}P-MRS

Human subjects underwent ^{31}P dynamic MRS scanning of the lower limb, specifically the tibialis anterior muscle, during exercise. Scans were acquired at a 2 min resting baseline prior to 30 seconds of exercise followed by 10 minutes recovery. Dynamometer exercise in the tibialis anterior muscle was performed using a custom- built MR compatible ergometer. ^{31}P dynamic spectra (Supplementary Figure 1) were acquired on a 3T MRI scanner (MR750, GE HealthCare, Waukesha, WI, USA) using a ^{31}P/^{1}H dual tuned transmit-receive surface coil (RAPID Biomedical GmbH, Rimpar, Germany). An unlocalized MRS sequence was used to acquire the dynamic spectra; repetition time (TR) = 2000 ms, flip angle (FA) = 70º, repetitions = 360, total acquisition time of 12 min. Data was acquired with 1024 samples at a bandwidth of 5 kHz, corresponding to a spectral resolution of 5 Hz (0.09 ppm). Phosphorus metabolites were determined with Advanced Method for Accurate, Robust, and Efficient Spectral (AMARES) fitting using OXSA (*39*), an open-source magnetic resonance spectroscopy analysis toolbox in MATLAB. An example of AMARES fitted spectra from the acquired temporal spectra is shown in Supplementary Figure 1. Phosphorus spectra were analyzed in MATLAB R2020a (MathWorks, Natick, MA, USA) using the MNS Research Pack created by GE HealthCare. Aerobic muscle load was determined with a pH decrease below 0.5 during exercise using the chemical shift difference of inorganic phosphorus (Pi) and PCr, as previously described (*40*): $\mathrm{pH} = 6.75 + \log\left(\frac{\delta - 3.27}{5.69 - \delta}\right)$. where δ is the ppm difference between PCr and inorganic phosphate as determined through AMARES. Following the recommendations of the 31P MRS in Skeletal Muscle Expert's Consensus recommendations (*41*), ATP was used as an internal concentration standard assumed constant at 8.2 mM; and the time constant of the phosphocreatine (PCr) recovery following a mono-exponential fit was determined using a least squares minimization algorithm to the expression

$$\mathrm{PCr(t)} = \mathrm{PCr_0} + C\left(1 - e^{\frac{-t}{\tau}}\right),$$

where PCr_0 is the PCr level at the end of recovery, C is the difference between exercise and recovery end (sometimes called Δ[PCr]), and τ is the time constant of PCr resynthesis in seconds, a measure of oxidative capacity. From these data, the estimated initial rate of PCr resynthesis was defined as $V_{\mathrm{iPCr}} = \Delta\mathrm{PCr}/\tau$, and Q_{max}, the maximal rate of oxidative ATP synthesis from the PCR recovery data, i.e. a measure of mitochondrial capacity, was determined by a model taking into account the Michaelis-Menten dependence of oxidative metabolism on the concentration of ADP (*42*); through the relation

$$[\mathrm{ADP}] = \frac{[\mathrm{Cr}][\mathrm{ATP}]}{[\mathrm{PCr}][\mathrm{H^+}]K_{\mathrm{CK}}},$$

where this relation is solved subject to the assumption of a constant concentration of total creatine, [tCr] ≈ 42 mM and utilizing knowledge of the Michaelis-Menten coefficient $K_{\mathrm{CK}} \approx 1.66 \times 10^9\ \mathrm{M}^{-1}$ (*42*). Finally, Q_{max} was estimated assuming a constant Michaelis-Menten $K_M \approx 30$ μM for the oxidation of ADP, empirically valid in skeletal muscle (*42*, *43*) according to the relation

$$Q_{\mathrm{max}} = V_{\mathrm{iPCr}}\left(1 + \frac{K_M}{[\mathrm{ADP}]_{\mathrm{End\ of\ exercise}}}\right)$$

Statistical Analysis

Data are presented as mean ± SEM unless otherwise stated. Statistical analysis was performed using GraphPad Prism software (version 10.1.0). Normality of data distribution was examined, and parametric and non-parametric tests were used accordingly. Comparison between two groups was performed by Student's t-test, with Welch's correction for unequal variance applied accordingly, or Mann-Whitney U test used when data were non-normally distributed. Comparison of two or more groups was performed by one-way analysis of variance (ANOVA) using Tukey's correction for multiple comparisons where applicable. A two-way ANOVA was used when two factors were present, post-hoc analysis was completed dependent on whether a significant interaction or main effect was found. Differences were considered significant when $p < 0.05$.

List of Supplementary Materials

Figs. S1 to S7

Tables S1 to S3

References and Notes

1. C. P. Kovesdy, Epidemiology of chronic kidney disease: an update 2022. *Kidney Int Suppl (2011)* **12**, 7-11 (2022).
2. "Kidney disease: A UK public health emergency," (Kidney Research UK, 2023).
3. J. Jankowski, J. Floege, D. Fliser, M. Bohm, N. Marx, Cardiovascular Disease in Chronic Kidney Disease: Pathophysiological Insights and Therapeutic Options. *Circulation* **143**, 1157-1172 (2021).
4. N. Patel, M. M. Yaqoob, D. Aksentijevic, Cardiac metabolic remodelling in chronic kidney disease. *Nat Rev Nephrol* **18**, 524-537 (2022).
5. K. Smith, D. Semple, D. Aksentijevic, S. Bhandari, A. M. Seymour, Functional and metabolic adaptation in uraemic cardiomyopathy. *Front Biosci (Elite Ed)* **2**, 1492-1501 (2010).
6. A. M. Chesser, S. M. Harwood, M. J. Raftery, M. M. Yaqoob, Myocardial bioenergetic abnormalities in experimental uremia. *Int J Nephrol Renovasc Dis* **9**, 129-137 (2016).
7. T. D. Nguyen, P. C. Schulze, Cardiac Metabolism in Heart Failure and Implications for Uremic Cardiomyopathy. *Circ Res* **132**, 1034-1049 (2023).
8. C. Zoccali *et al.*, The systemic nature of CKD. *Nat Rev Nephrol* **13**, 344-358 (2017).
9. Y. Li *et al.*, Energy Metabolism Dysregulation in Chronic Kidney Disease. *Kidney360* **4**, 1080-1094 (2023).
10. K. Heitman, M. S. Alexander, C. Faul, Skeletal Muscle Injury in Chronic Kidney Disease-From Histologic Changes to Molecular Mechanisms and to Novel Therapies. *Int J Mol Sci* **25**, (2024).
11. P. Romagnani *et al.*, Chronic kidney disease. *Nat Rev Dis Primers* **3**, 17088 (2017).
12. L. Orlic *et al.*, Chronic kidney disease and nonalcoholic Fatty liver disease-is there a link? *Gastroenterol Res Pract* **2014**, 847539 (2014).
13. C. K. Yeung, D. D. Shen, K. E. Thummel, J. Himmelfarb, Effects of chronic kidney disease and uremia on hepatic drug metabolism and transport. *Kidney Int* **85**, 522-528 (2014).

14. A. Chapagain *et al.*, Elevated hepatic 11beta-hydroxysteroid dehydrogenase type 1 induces insulin resistance in uremia. *Proc Natl Acad Sci U S A* **111**, 3817-3822 (2014).

15. D. Aksentijevic, The University of Hull, https://hull-repository.worktribe.com/output/4212871 (2008).

16. D. Aksentijevic, S. Bhandari, A.-M. Seymour, Altered expression of myocardial [Ca2+] handling proteins in experimental uraemia. *Journal of Molecular and Cellular Cardiology* **42**, (2007).

17. D. Aksentijevic, S. Bhandari, A. M. Seymour, Insulin resistance and altered glucose transporter 4 expression in experimental uremia. *Kidney Int* **75**, 711-718 (2009).

18. A. E. Raine, A. M. Seymour, A. F. Roberts, G. K. Radda, J. G. Ledingham, Impairment of cardiac function and energetics in experimental renal failure. *J Clin Invest* **92**, 2934-2940 (1993).

19. D. Aksentijevic *et al.*, Intracellular sodium elevation reprograms cardiac metabolism. *Nat Commun* **11**, 4337 (2020).

20. Y. Honda *et al.*, Chronic kidney disease is a key predictive factor for potential myocardial ischaemia and poor prognosis in asymptomatic patients with diabetes mellitus. *Sci Rep* **12**, 10268 (2022).

21. D. Taylor, S. Bhandari, A. M. Seymour, Mitochondrial dysfunction in uremic cardiomyopathy. *Am J Physiol Renal Physiol* **308**, F579-587 (2015).

22. S. F. Parnham, J. M. Gleadle, C. G. De Pasquale, J. B. Selvanayagam, Myocardial Ischemia Assessment in Chronic Kidney Disease: Challenges and Pitfalls. *Front Cardiovasc Med* **1**, 13 (2014).

23. C. Zoccali, G. Tripepi, E. Dounousi, F. Mallamaci, Chronic Kidney Disease (CKD) as a Systemic Disease: Whole Body Autoregulation and Inter-Organ Cross-Talk. *Kidney and Blood Pressure Research* **39**, 134-141 (2014).

24. B. Roshanravan, J. Gamboa, K. Wilund, Exercise and CKD: Skeletal Muscle Dysfunction and Practical Application of Exercise to Prevent and Treat Physical Impairments in CKD. *Am J Kidney Dis* **69**, 837-852 (2017).

25. A. S. Ryan, Role of Skeletal Muscle Mitochondrial Dysfunction in CKD. *Clin J Am Soc Nephrol* **15**, 912-913 (2020).

26. D. Durozard *et al.*, 31P NMR spectroscopy investigation of muscle metabolism in hemodialysis patients. *Kidney Int* **43**, 885-892 (1993).

27. T. Thome *et al.*, Impaired muscle mitochondrial energetics is associated with uremic metabolite accumulation in chronic kidney disease. *JCI Insight* **6**, (2021).

28. T. Thome *et al.*, Uremic metabolites impair skeletal muscle mitochondrial energetics through disruption of the electron transport system and matrix dehydrogenase activity. *American Journal of Physiology-Cell Physiology* **317**, C701-C713 (2019).

29. M. Rao, B. L. Jaber, V. S. Balakrishnan, Chronic kidney disease and acquired mitochondrial myopathy. *Curr Opin Nephrol Hypertens* **27**, 113-120 (2018).

30. L. Orlić *et al.*, Chronic Kidney Disease and Nonalcoholic Fatty Liver Disease—Is There a Link? *Gastroenterology Research and Practice* **2014**, 847539 (2014).

31. T. J. Hydes *et al.*, The impact of non-alcoholic fatty liver disease and liver fibrosis on adverse clinical outcomes and mortality in patients with chronic kidney disease: a prospective cohort study using the UK Biobank. *BMC Med* **21**, 185 (2023).

32. S. Baliou *et al.*, Protective role of taurine against oxidative stress (Review). *Mol Med Rep* **24**, (2021).

33. S. Strocchi *et al.*, Systems Biology Approach Uncovers Candidates for Liver-Heart Interorgan Crosstalk in HFpEF. *Circ Res* **135**, 873-876 (2024).

34. Y. Oishi, I. Manabe, Organ System Crosstalk in Cardiometabolic Disease in the Age of Multimorbidity. *Front Cardiovasc Med* **7**, 64 (2020).

35. V. Diwan, L. Brown, G. C. Gobe, Adenine-induced chronic kidney disease in rats. *Nephrology (Carlton)* **23**, 5-11 (2018).

36. C. G. Faulkes *et al.*, Naked mole-rats have distinctive cardiometabolic and genetic adaptations to their underground low-oxygen lifestyles. *Nat Commun* **15**, 2204 (2024).

37. D. Aksentijevic, H. R. Lewis, M. J. Shattock, Is rate-pressure product of any use in the isolated rat heart? Assessing cardiac 'effort' and oxygen consumption in the Langendorff-perfused heart. *Exp Physiol* **101**, 282-294 (2016).

38. L. McClements *et al.*, Impact of reduced uterine perfusion pressure model of preeclampsia on metabolism of placenta, maternal and fetal hearts. *Sci Rep* **12**, 1111 (2022).

39. L. A. B. Purvis *et al.*, OXSA: An open-source magnetic resonance spectroscopy analysis toolbox in MATLAB. *PLoS One* **12**, e0185356 (2017).

40. I. R. Lanza, D. M. Wigmore, D. E. Befroy, J. A. Kent-Braun, In vivo ATP production during free-flow and ischaemic muscle contractions in humans. *J Physiol* **577**, 353-367 (2006).

41. M. Meyerspeer *et al.*, (31) P magnetic resonance spectroscopy in skeletal muscle: Experts' consensus recommendations. *NMR Biomed* **34**, e4246 (2020).

42. L. Valkovic, M. Chmelik, M. Krssak, In-vivo(31)P-MRS of skeletal muscle and liver: A way for non-invasive assessment of their metabolism. *Anal Biochem* **529**, 193-215 (2017).

43. G. J. Kemp, G. K. Radda, Quantitative interpretation of bioenergetic data from 31P and 1H magnetic resonance spectroscopic studies of skeletal muscle: an analytical review. *Magn Reson Q* **10**, 43-63 (1994).

Acknowledgments:

We would like to thank Dr Nasima Kanwal and School of Physical and Chemical Sciences NMR Facility, Queen Mary University of London. DA is a co-PI of Barts Metabolism Network.

Funding:

Wellcome Trust Career Re-Entry Fellowship 221604/Z/20/Z (DA)

Barts Charity grant G-002145 (DA)

British Heart Foundation MRes Studentship FS/4YPhD/P/20/34016 (NP)

Barts HCA Fellowship (LK)

Leventis Foundation Cyprus (LK)

Novo Fonden grant NNF21OC0068683 (MA, JJM, CL, MV)

MRC MDU Mouse Biochemistry Laboratory MC_UU_00014/5

Centre of Excellence in Medical Engineering funded by Wellcome Trust (TRE)

EPSRC WT/203148/Z/16/Z (TRE)

BHF Centre of Research Excellence RE/18/2/34213 (TRE)

Wellcome Trust Sir Henry Dale Fellowship 221805/Z/20/Z (LV)

Slovak grant agencies VEGA 2/0004/23 and APVV 21-0299 (LV)

Author contributions:

Conceptualization: DA, MMY, NHB, CL

Methodology: DA, MY, MA, NP, FC, ESSH, JEC, TRE, MV, LK, LV, JJJJM, NHB, CL

Investigation: DA, MY, MA, NP, FC, ESSH, JEC, TRE, MV, LK, LV, JJJJM, NHB

Visualization: MY, DA, MA

Funding acquisition: DA, MMY, CL, NHB

Project administration: DA

Supervision: DA, MMY, JJJJM, NHB, CL

Writing – original draft: MY, MA, DA

Writing – review & editing: MY, DA, MMY, JJJJM, MA, ESSH, TRE, MV, LV, NHB, CL

Competing interests: None.

Data and materials availability: Data available on reasonable request from the corresponding author.

Table 1. Plasma analysis of adenine diet-CKD and chow diet controls. Analysed by Student t-test, *p<0.05 vs. Control.

	Control (n=8)	Adenine CKD (n=10)
Glucose (mmol/L)	13.20 ± 0.35	**10.01 ± 0.36***
Sodium (mmol/L)	142.1 ± 0.44	140.7 ± 1.17
Potassium (mmol/L)	4.98 ± 0.21	**6.58 ± 0.32***
Chloride (mmol/L)	95.13 ± 0.69	96.40 ± 1.62
Triglycerides (mmol/L)	1.27 ± 0.28	0.82 ± 0.07
Insulin (µg/L)	1.83 ± 0.24	**0.54 ± 0.11***
Free Fatty Acids (µmol/L)	337.6 ± 62.21	224.2 ± 34.01
Alanine aminotransferase (U/L)	40.14 ± 2.48	39.89 ± 2.64
Alkaline Phosphatase (U/L)	99.00 ± 8.11	**125.7 ± 8.99***

Table 2. Plasma analysis of PN CKD and sham controls. Analysed by Student t-test, *p<0.05 vs. Sham.

	Sham (n=7)	PN CKD (n=7)
Glucose (mmol/L)	8.3 ± 0.65	7.64 ± 0.27
Sodium (mmol/L)	138.9 ± 1.01	138.8 ± 0.4
Potassium (mmol/L)	4.87 ± 0.18	5.58 ± 0.39
Chloride (mmol/L)	92.43 ± 1.66	94.0 ± 0.72
Triglycerides (mmol/L)	1.5 ± 0.18	1.25 ± 0.21
Insulin (µg/L)	0.79 ± 0.44	0.44 ± 0.07
Free Fatty Acids (µmol/L)	790.1 ± 142	757.6 ± 156
Alanine aminotransferase (U/L)	43.43 ± 3.68	**32.33 ± 2.41***
Alkaline Phosphatase (U/L)	85.57 ± 5.55	78.14 ± 7.13

Table 3. Demographics of CKD patients and healthy controls. Data displayed as mean ± SD. *Most recent values, **All treated with antihypertensive medication. eGFR: estimated Glomerular Filtration Rate, UACR: Urine-Albumin-Creatinine-ratio, ANCA: anti-neutrophilocyte-cytoplasmic-antibody, ADPKD: autosomal dominant polycystic kidney disease

	Healthy controls, (n=5)	n, number of values	CKD patients, (n=10)	n, number of values
Age (years)	54 ± 12	5	61.40 ± 11.68	10
Gender, n (%)		5		10
- Male	4 (80%)		8 (80%)	
- Female	1 (20%)		2 (20%)	
Height (cm)	176 ± 8.4	5	174.6 ± 9.914	9
Weight (kg)	80 ± 14	5	88.30 ± 19.73	10
Biochemistry of non-diabetic CKD patients*				
eGFR (ml/min/1.73 m^2)			26.60 ± 7.37	10
- eGFR 45-35			38 ± 1.41	2
- eGFR <35-25			27 ± 1.58	5
- eGFR <25			18.33 ± 2.30	3
UACR (mg/g)			421.9 ± 327.1	10
- UACR >1000			1191	1
- UACR <1000-500			524.2 ± 21.92	2
- UACR <500-100			313.8 ± 186.5	6
- UACR <100			96	1
Medical history of non-diabetic CKD patients				
Hypertension, n (%)				10
Yes**			9 (90%)	
No			1 (10%)	
Aetiology, n (%)				10
Hypertensive nephropathy			4 (40%)	
ANCA-associated vasculitis			2 (20%)	
Obstructive nephropathy			1 (10%)	
ADPKD			1 (10%)	
Sequelae after acute kidney failure (due to sepsis)			1 (10%)	
CKD of unknown cause			1 (10%)	
Stage of CKD, n (%)				10
CKD stage 3b			2 (20%)	
CKD stage 4			8 (80%)	
Duration of illness with eGFR<60, n (%)				10
5-10 years			3 (30%)	
>10 years			7 (70%)	

Figures

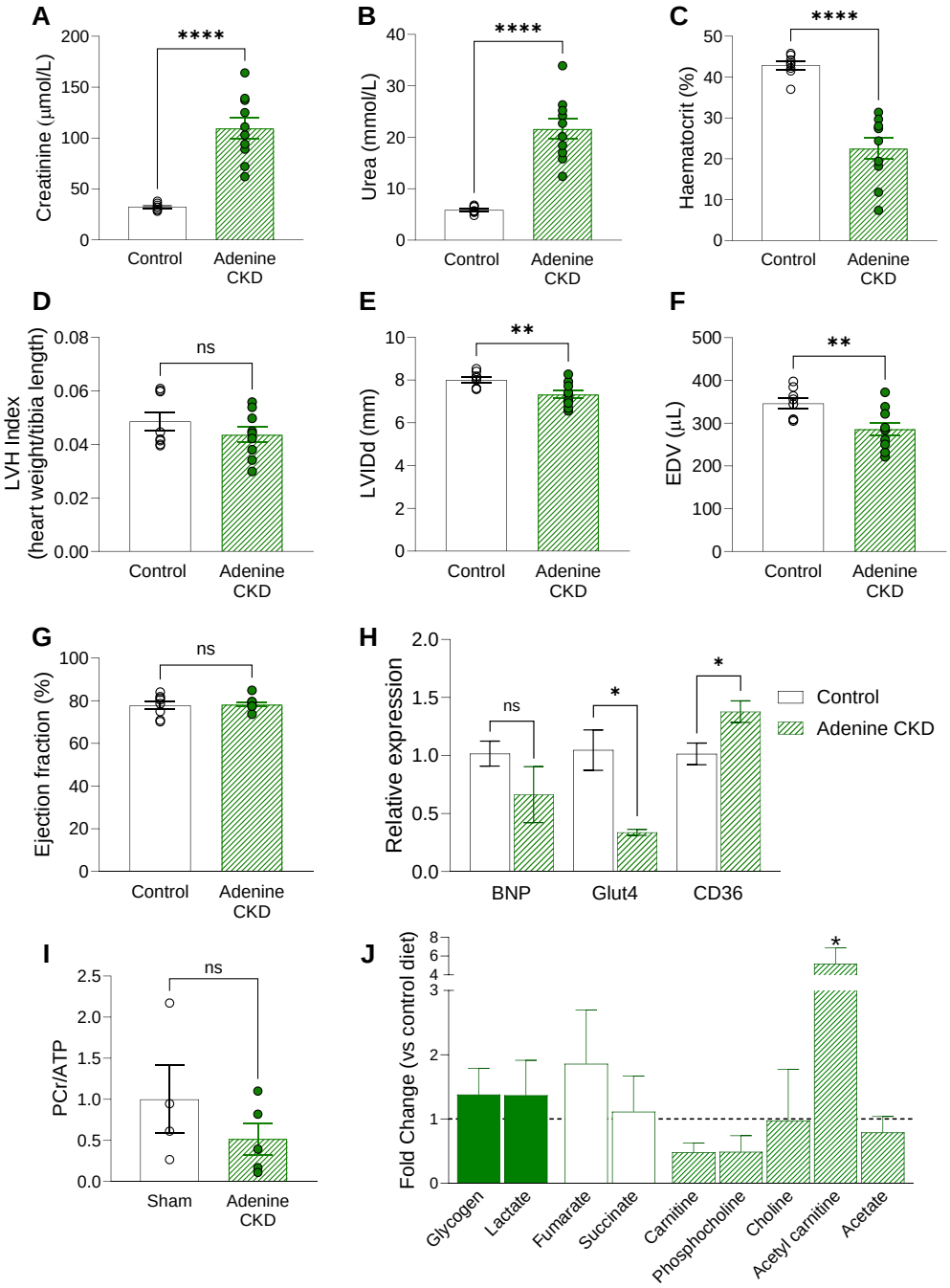

Fig. 1. Morphological and cardiac metabolic changes in adenine diet CKD model. (**A-B**) Plasma levels of creatinine and urea (Adenine n=10, control n=8, unequal variance t-test, *p<0.05). (**C**) Haematocrit measurement (Adenine n=10, control n=8, unequal variance t-test, *p<0.05). (**D**) ratio of

heart weight to tibia length (Adenine=10, control n=8, Student's t-test, *p<0.05), (**E-G**) Echocardiography measurement of left ventricle internal diameter in diastole (LVID,d), end diastolic volume (EDV) and ejection fraction (Adenine=10, control n=8, Student's t-test, *p<0.05). (**H**) mRNA expression of BNP, Glut4 and CD36 relative to housekeeping gene 36B4 (Adenine n=5, control n=4. BNP analysed by Mann-Whitney U test, Glut4 analysed by unequal variance t-test and CD36 analysed by Students t-test, *p<0.05). (**I**) Ratio of PCr/ATP measured by ^{1}H NMR spectroscopy in cardiac tissue from adenine CKD (n=5) and control diet (n=4) animals. Analysed by Student's t-test, *p<0.05. (**J**) ^{1}H NMR spectroscopy of cardiac tissue from adenine CKD (n=5) expressed as fold change vs control diet (n=4) group. Adenine CKD vs control compared for each metabolite by Student's t-test, *p<0.05.

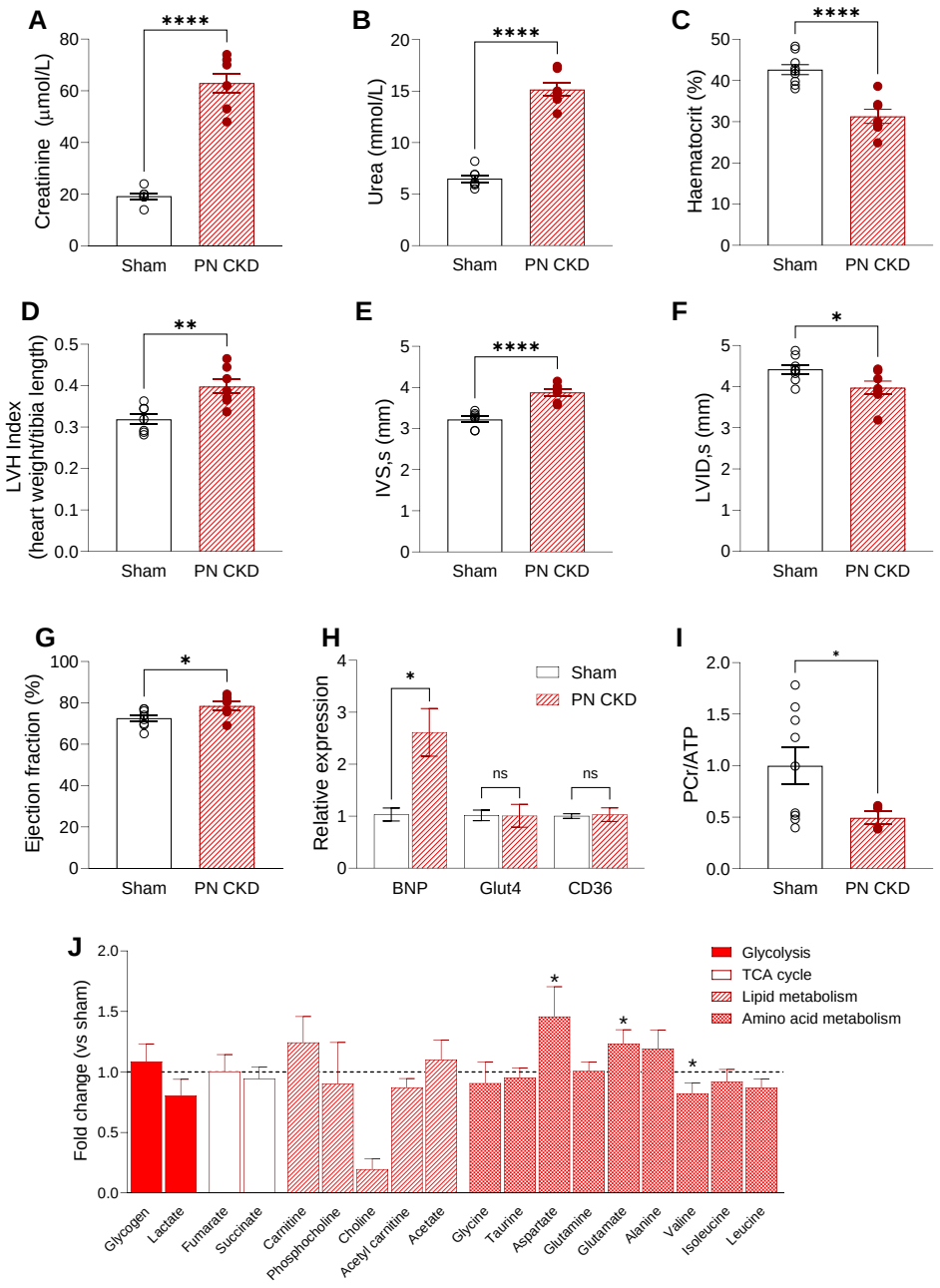

Fig. 2. CKD phenotype and cardiometabolic remodelling in PN CKD model. (**A-B**) Plasma levels of creatinine and urea (PN CKD n=7, sham n=7, Students t-test, *p<0.05). (**C**) Haematocrit measurement (PN CKD n=7, sham n=9, Students t-test, *p<0.05). (**D**) ratio of heart weight to tibia length (PN CKD n=7, sham n=7, Student's t-test, *p<0.05. (**E-G**) Echocardiography measurement of intraventricular

septum thickness in systole (IVS,s), left ventricle internal diameter in systole (LVID,s) and ejection fraction (PN CKD n=7, sham n=8, Student's t-test, *p<0.05). (**H**) mRNA expression of BNP, Glut4 and CD36 relative to housekeeping gene 36B4 (PN CKD n=5, sham n=5. BNP analysed by unequal variance t-test, Glut4 and CD36 analysed by Student's *t*-test, *p<0.05). (**I**) Ratio of PCr/ATP measured by ^{1}H NMR spectroscopy in cardiac tissue from PN CKD (n=5) and sham (n=9) animals. Analysed by unequal variance t-test, *p<0.05. (**J**) ^{1}H NMR spectroscopy of cardiac tissue from PN CKD (n=5) expressed as fold change vs sham group (n=9). PN CKD vs sham compared for each metabolite by Student's t-test, *p<0.05.

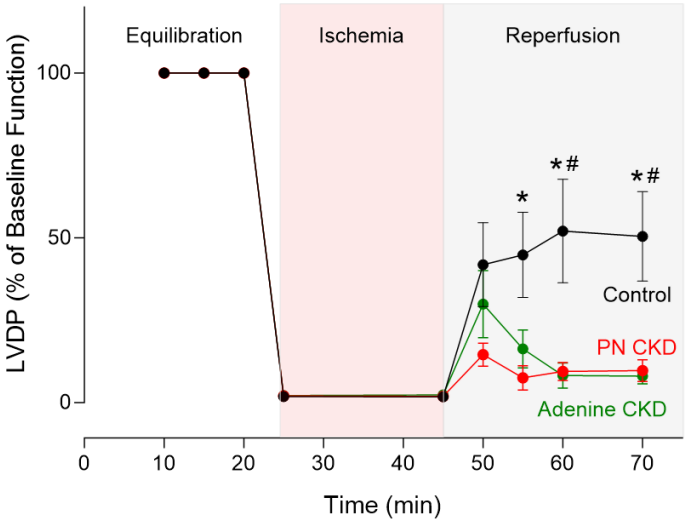

Fig. 3. Ischemia and reperfusion in CKD hearts. Functional recovery in PN CKD (n=4), adenine CKD (n=5) and control hearts (n=5). Left ventricle developed pressure (LVDP) displayed as a percentage of baseline value. Analysed by two-way repeated measures ANOVA, significant interaction (p<0.05) between groups over time. One-way ANOVA analysis for each time point displayed, *p<0.05 PN CKD vs. control, #p<0.05 Adenine CKD vs. control.

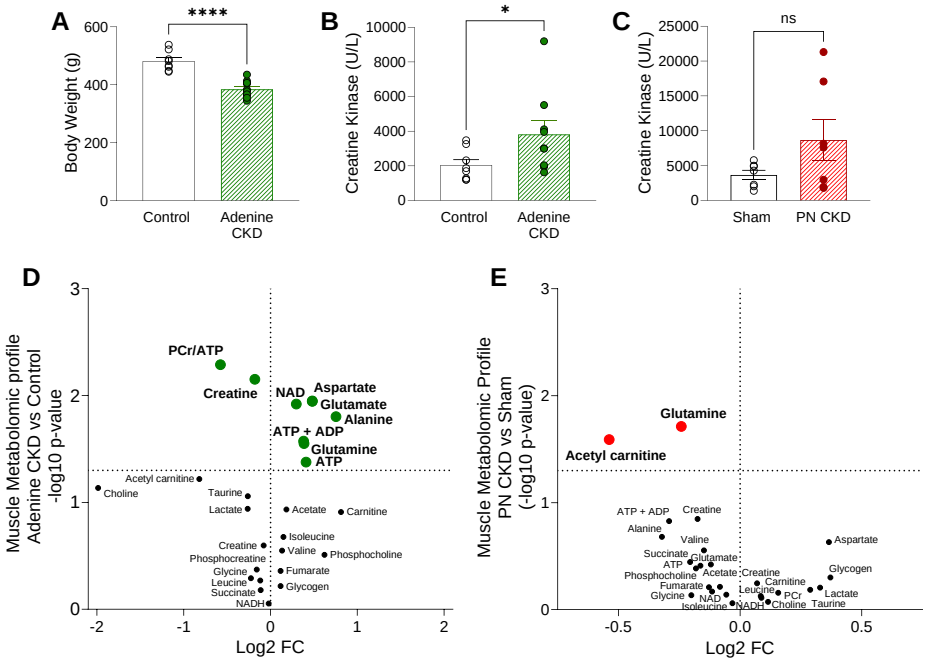

Fig. 4. Metabolomic profile of skeletal muscle in adenine and PN CKD models. (**A**) Terminal body weight in adenine CKD animals. Analysed by Students t-test, *p<0.05, control n=8, Adenine n=10 (**B-C**) Plasma creatine kinase level in (B) adenine diet CKD animals (Analysed by Mann-Whitney U test, *p<0.05, control n=8, Adenine n=10) and (C) PN CKD animals (Analysed by unequal variance t-test, p>0.05, sham n=8, PN CKD n=8). (**D-E**) Muscle metabolomic profile measured by ^{1}H NMR spectroscopy of (D) adenine diet CKD (n=5) vs control diet (n=5) and (E) PN CKD (n=3) vs sham (n=3). Each point represents the fold change (FC) of a metabolite plotted against the associated level of statistical significance for the change analysed by t-test (horizontal dashed line indicates p=0.05 threshold).

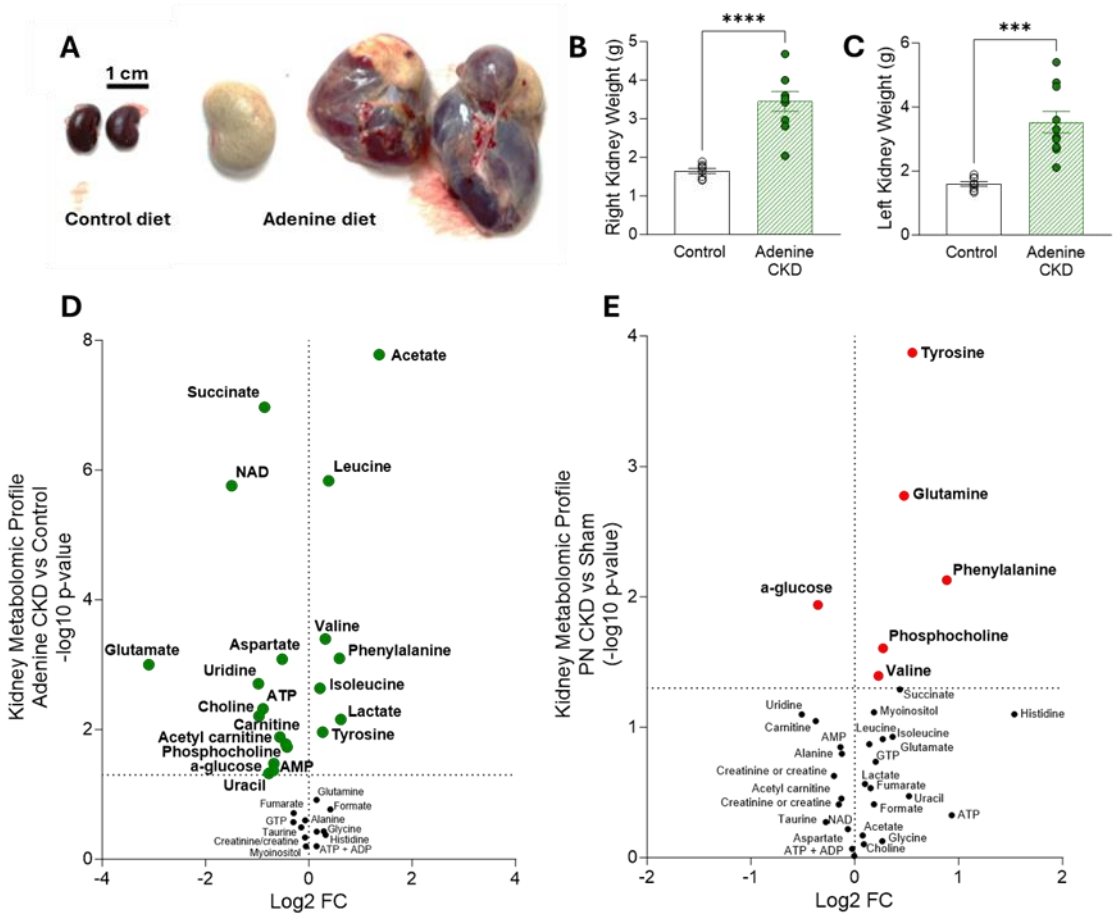

Fig. 5. Kidney morphology and metabolomic profile of adenine and PN CKD models. (**A**) Representative images of adenine CKD and control kidneys. (**B-C**) Right and left kidney weight. Analysed by unequal variance t-test, *p<0.05, control n=8, Adenine n=10. (**D-E**) Kidney metabolomic profile measured by ^{1}H NMR spectroscopy of (D) adenine diet CKD (n=5) vs control diet (n=9) and (E) PN CKD (n=4) vs sham (n=4). Each point represents the fold change (FC) of a metabolite plotted against the associated level of statistical significance for the change analysed by t-test (horizontal dashed line indicates p=0.05 threshold).

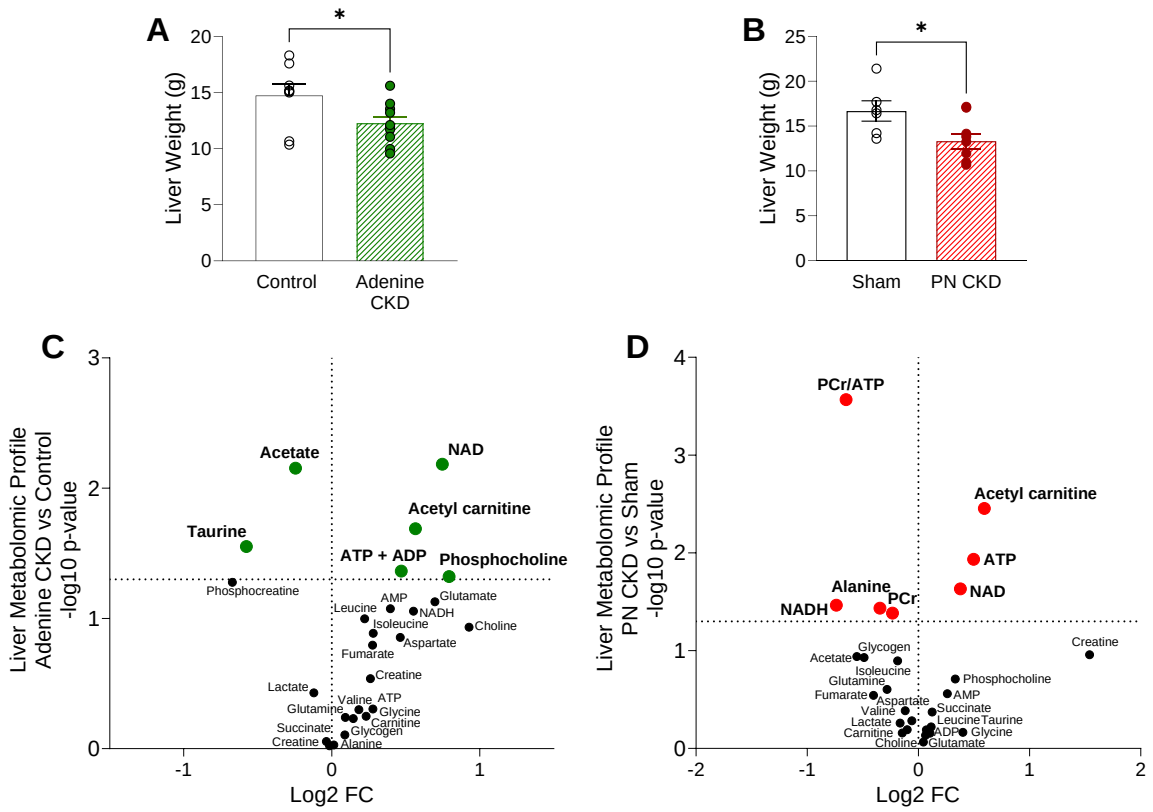

Fig. 6. Metabolomic profile of liver in adenine and PN CKD models. (**A-B**) Liver weight in (A) adenine diet CKD (n=10) vs control diet (n=8) animals and (B) PN CKD (n=9) and sham (n=6) animals. Analysed by Student's t-test, *p<0.05. (**C-D**) Liver metabolomic profile measured by ^{1}H NMR spectroscopy of (C) adenine diet CKD (n=5) vs control diet (n=4) and (D) PN CKD (n=4) vs sham (n=4). Each point represents the fold change (FC) of a metabolite plotted against the associated level of statistical significance for the change analysed by t-test (horizontal dashed line indicates p=0.05 threshold).

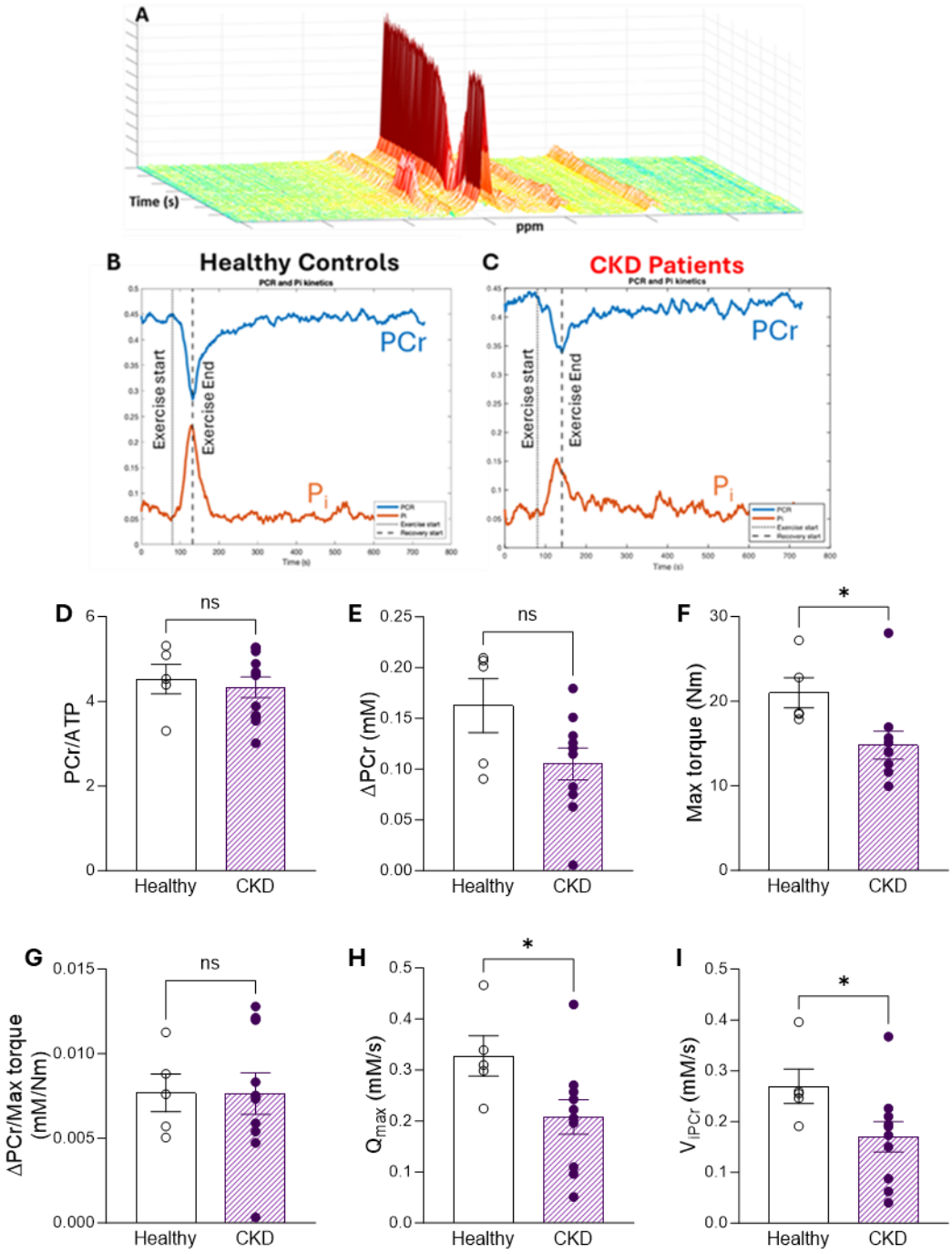

Fig. 7. Human ^{31}P MRS in tibialis anterior muscle of healthy controls and CKD patients during exercise. (**A**) Dynamic ^{31}P spectra. (**B-C**) Change in PCr and Pi before, during and after 30 seconds of exercise. (**D**) Baseline PCr levels, (**E**) ΔPCr (difference in PCr between rest and end of exercise), (**F**) Maximum torque generation during exercise and (**G**) ΔPCr normalised to maximum torque generation in

CKD patients and healthy controls. (**H**) Estimated mitochondrial capacity for maximal ATP resynthesis (Q_{max}), determined as described in the text. (**I**) Estimated initial rate of PCr resynthesis following exercise as described in the test. (D-I) *$p<0.05$, healthy controls n=5, CKD patients n=10. (D, G-H) Analysed by unequal variance *t*-test, (E-F, I) analysed by Mann-Whitney U test.